RSC Advances

ROYAL SOCIETY OF CHEMISTRY

www.rsc.org/advances

RSC Advances

ARTICLE

A fluorescent nanoprobe based on metal enhanced fluorescence combined with Förster resonance energy transfer for the trace detection of nitrite ion

Received 00th January 20xx,
Accepted 00th January 20xx

DOI: 10.1039/x0xx00000x

www.rsc.org/

Yong-liang Liu[a], Ning Kang[a], Xue-bin Ke[a], Dong Wang[a], Lei Ren*[ab] and Hong-jun Wang[c]

Fluorescent nanoprobes have been investigated for detection of nitrite ion. However, the fluorescence intensity and sensitivity of fluorescent nanoprobes were still restricted by their low quantum yield. A novel fluorescent nanoprobe based on metal enhanced fluorescence combined with Förster resonance energy transfer was developed for the trace detection of NO_2^- in this work. 24.8-fold fluorescence enhancement of CdTe QDs was achieved with exact control over the size of Au nanospheres and the thickness of silica shell between the Au NSs and CdTe Quantum dots in the Au@SiO_2-CdTe nanoparticles, and coating Au@SiO_2-CdTe NPs with denatured bovine serum albumin. The detection of NO_2^- with the obtained Au@SiO_2-CdTe@dBSA-neutral red fluorescent nanoprobe was based on the FRET from CdTe QDs to neutral red. The detection limit of NO_2^- in aqueous solution was found to be as low as 60 nM, much lower than the maximum permitted concentration of 2.2 μM in drink water. In addition, Au@SiO_2-CdTe@dBSA-NR fluorescent nanoprobe was successfully applied to the detection of NO_2^- in real samples and cells supernatants with precise and accurate results.

1 Introduction

Nitrite, as fertilizing and preservative agents for food, widely exists in the environment. The increasing concentration of nitrite in water resource and food products is causing serious concerns to public health and environmental safety. Nitrite can form some carcinogens compounds such as N-nitrosamines by reacting with amine.[1] Moreover, nitric oxide (NO) plays an important role in the regulation of immunological responses *in vivo*,[2, 3] and NO can be easily oxidized to nitrite in aqueous solution and in the body.[4] Therefore, the quantitative detection of nitrite ion (NO_2^-) is extremely urgent in water sources, food products and bio-samples. To date, a considerable number of approaches have been developed for the detection of NO_2^-, such as chemiluminescence,[5, 6] chromatography,[7, 8] capillary electrophoresis[9] and electrochemistry methods.[10] However, most of these methods are restricted by long consuming time, complicated and expensive instrumental cost. Compared with these methods, fluorescent nanoprobes possess the advantages of low cost, high speed and low limit of detection.[11, 12] Nevertheless, fluorescent nanoprobes still suffer from low quantum yield, resulting in weak fluorescence intensity and low sensitivity. Thus, it is of great desire to develop fluorescent nanoprobes with high sensitivity and selectivity for the detection of NO_2^-.

Noble metal nanoparticles (NPs), such as Au and Ag NPs, can enhance the local electromagnetic field surrounding them and finally result in fluorescence enhancement of nearby organic dyes or quantum dots (QDs). This phenomenon is broadly termed as metal enhanced fluorescence (MEF),[13, 14] in which the size of metal NPs and the distance between metal NPs and fluorescence molecules are key factors for enhancement effects. MEF has been investigated to increase the sensitivity of fluorescent nanoprobes, such as QDs nanoprobes[15, 16] and upconversion fluorescent nanoprobes.[17] Furthermore, Förster resonance energy transfer (FRET), a phenomenon between donor and acceptor molecules,[18, 19] has also been utilized to improve the sensitivity of nanoprobes combined with MEF.[20, 21] For instance, Asselin *et al*, synthesized multi-shell metal/silica NPs based on MEF and FRET, which were successfully applied to the ultrasensitive and sequence-specific sensing of minute amounts of DNA without any labeling or amplification of the nucleic acids.[20] Kochuveedu *et al*, developed a multilayer core-shell nanostructure consisting of an Au core and surrounding FRET pairs, i.e., CdSe quantum dot donors and Sulforhodamine101 (S101) dye acceptors.[21] The multilayer configuration was demonstrated to exhibit synergistic effects of surface plasmon energy transfer from the metal to the CdSe and plasmon-enhanced FRET from the QDs to the dye. Moreover, denatured bovine serum albumin (dBSA), a kind of BSA protein with special structure, was used to enhance the fluorescence intensity and stability of QDs.[22, 23] However, as far as

[a]*Department of Biomaterials, College of Materials, Xiamen University, Xiamen 361005, People's Republic of China. E-mail: renlei@xmu.edu.cn; Fax: +86-5922183937; Tel: +86-5922188530*
[b]*State Key Laboratory for Physical Chemistry of Solid Surfaces, Department of Chemistry, College of Chemistry and Chemical Engineering, Xiamen University, Xiamen, 361005, People's Republic of China*
[c]*Department of Chemistry, Chemical Biology and Biomedical Engineering, Stevens Institute of Technology, 1 Castle Point on Hudson, Hoboken, New Jersey, 07030, USA*

we know, fluorescent nanoprobes utilizing MEF, FRET and modifying with dBSA for the detection of NO_2^- have not been reported yet.

In the present work, a novel fluorescent nanoprobe based on MEF combined with FRET was developed for the trace detection of NO_2^-. With the precise control over the size of Au nanospheres (NSs) and the distance between Au NSs and CdTe QDs by varying the thickness of the silica shell, the fluorescence intensity of CdTe QDs was significantly enhanced based on MEF. Subsequently, the fluorescence intensity was further improved by coating Au@SiO_2-CdTe NPs with denatured dBSA, which could also provide binding site for neutral red (NR), a reagent for the spectrophotometric determination of NO_2^-.[24, 25] The obtained Au@SiO_2-CdTe@dBSA-NR fluorescent nanoprobe could selectively detect NO_2^- and the detection mechanism was discussed. In addition, Au@SiO_2-CdTe@dBSA-NR fluorescent nanoprobe was successfully applied to the detection of NO_2^- in water and meat food samples and lipopolysaccharide (LPS)-induced RAW 246.7 cells supernatants with precise and accurate results. The as-prepared Au@SiO_2-CdTe@dBSA-NR fluorescent nanoprobes exhibited high selectivity, sensitivity and low detection limit, revealing the potential application of fluorescent nanoprobes based on MEF combined with FRET.

2. Experimental section

2.1 Materials

Chloroauric acid trihydrate ($HAuCl_4 \cdot 3H_2O$), sodium citrate, cetyltrimethyl ammonium bromide (CTAB), sodium hydroxide (NaOH), hydrochloric acid (HCl), tetraethoxysilane (TEOS), L-ascorbic acid (AA), cadmium chloride hydrate ($CdCl_2 \cdot 2.5H_2O$), sodium nitrate ($NaNO_3$), sodium bicarbonate ($NaHCO_3$), sodium dihydrogen phosphate (NaH_2PO_4), disodium hydrogen phosphate (Na_2HPO_4), sodium sulfate (Na_2SO_4), sodium chloride (NaCl), ammonium nitrate (NH_4NO_3) and sodium fluoride (NaF) were purchased from Sinopharm Chemical Reagent Co., Ltd, (Shanghai, China). 3-aminopropyl trimethoxysilane (APTMS), thioglycolic acid (TGA), tellurium (Te) powder, N-hydroxysuccinimide (NHS), bovine serum albumin (BSA), 1-(3-dimethylaminopropyl)-3-ethylcarbodiimide hydrochloride (EDC·HCl), neutral red (NR) and lipopolysaccharide (LPS) were obtained from Sigma-Aldrich (Sigma-Aldrich St Louis, MO, USA). NO assay kit was purchased from Beyotime Biotechnology Co., Ltd, (Jiangsu, China). All of the reagents were analytical grade and used without further purification. Milli-Q water (18.2 MΩ) was used throughout the whole experiments.

2.2 Synthesis of Au NSs with different size

Au seeds were firstly synthesized using a slight modification of the seed-mediated approach reported by Frens et al.[26] Briefly, 100 mL of 2.5×10^{-4} M $HAuCl_4$ aqueous solution was transferred to a 250 mL three-necked round-bottom flask and heated to boiling under gentle stirring. 3.5 mL of 1% (wt/v) sodium citrate aqueous solution was then added all at once. The solution turned to wine red in several minutes. The boiling and stirring were continued for 20 min before cooling down to room temperature and kept at 4 ^oC for further use.

Au NSs with size ranging from 20 to 105 nm were prepared through a one-pot seed mediated process with CTAB as stabilizer.[27] In a typical procedure, 1 mL of 1% (wt/v) $HAuCl_4$ solution, 0.182 g of CTAB and 1 mL of 50 mM AA were added to a 250 mL conical flask. Then 2, 5, 10, 20 or 40 mL of as-prepared Au seed solution were added to the mixture, respectively. Each mixed solution were diluted to 100 mL and stirred for 6 h. Subsequently, 0.182 g of CTAB was added and allowed stirring for another 12 h, following by centrifugation at 5,500 rpm for 30 min twice, then re-dispersed in 10 mL of water.

2.3 Synthesis of different Au@SiO_2 NPs

Au@SiO_2 NPs were synthesized by a modified StÖber method.[28] By changing Au NSs or the dose of TEOS, a series of Au@SiO_2 NPs with same size of Au cores and different thickness of silica shell, or with different sizes of Au cores and same thickness of silica shell were obtained, respectively. Briefly, 2 mL of 5 nM Au NSs colloidal solution with different size were prepared. 0.1 M NaOH aqueous solution was added dropwise to adjust the pH to 10.0 under gentle stirring. Then 10 μL of 0.896 M TEOS methanol solution mixed with 12 μL of 0.114 M APTMS methanol solution was added to the mixture under stirring three times on 30-minute intervals. The mixed solution was gently stirred for 24 h and centrifuged at 5,500 rpm for 30 min twice and then re-dispersed in 10 mL of water.

2.4 Covalent binding of CdTe QDs to Au@SiO_2 NPs

Water-soluble TGA-capped CdTe QDs were prepared according to a synthetic route reported earlier.[29] The covalent binding of CdTe QDs to Au@SiO_2 NPs was performed using an EDC/NHS cross-linking procedure. In a typical experiment, 100 μL of 5 μM CdTe QDs solutions were pre-activated by 100 μL of 1 μM EDC solution mixed with 100 μL of 1 μM NHS solution for 1 h and then added to 10 mL colloidal solution of 1 nM Au@SiO_2 with different thickness of silica shell, respectively. The mixed solutions were gently shaken in dark at room temperature for 6 h. The unlinked CdTe QDs were separated by centrifugation at 5,600 rpm for 30 min twice. The final product was re-dispersed in 10 mL of water.

2.5 Preparation of Au@SiO_2-CdTe@dBSA NPs

dBSA was pre-prepared by treating BSA with $NaBH_4$ on the basis of previous literature reports.[30] Briefly, 100 mL of aqueous solution containing 0.33g BSA was prepared. 1 mL of 0.22 M $NaBH_4$ aqueous solution was injected under gentle stirring for 1 h at room temperature. The mixed solution was heated to 60-80 ^oC and kept for 20 min in water bath to decompose the excess $NaBH_4$.

0.5 mL of freshly prepared dBSA aqueous solution was added to 1 mL of 1 nM Au@SiO_2-CdTe solution. Then 100 μL of 1 μM EDC solution mixed with 100 μL of 1 μM NHS solution were injected. After shaking in dark at room temperature for 24 h, the mixed solution was centrifuged twice to remove the excess dBSA and then re-dispersed in 10 mL of water.

2.6 Electrostatic adsorption of NR to Au@SiO_2-CdTe@dBSA NPs

10 mL of 0.1 nM Au@SiO_2-CdTe@dBSA colloidal solution was prepared as described above. 1 mM HCl aqueous solution was added dropwise to adjust the pH to 6.0. Then 200 μL of 5 μM freshly prepared NR solution was injected. The mixed solution was shaken in dark at room temperature for 2 h and centrifuged twice at 5,600

rpm for 30 min. The obtained precipitation was re-dispersed in 10 mL of water.

2.7 NO_2^- detection in aqueous solution

The standard $NaNO_2$ solution in NO assay kit was diluted to 1, 2, 5, 10, 20, 40, 130 and 250 μM, respectively. 1 mL of 0.1 nM Au@SiO_2-CdTe@dBSA-NR colloidal solution were added with 200 μL of 0, 1, 2, 5, 10, 20, 40, 130 or 250 μM $NaNO_2$ solution, respectively and shaken for 2 min, respectively. Then all of the mixed solutions were diluted to 2 mL for the measurement.

Selectivity assay: 1 mL of 5 mM aqueous solutions containing a certain kind of ions (NO_2^-, Cl^-, HCO_3^-, $H_2PO_4^-$, F^-, NH_4^+, SO_4^{2-}, HPO_4^{2-} and NO_3^-) were prepared, respectively. Then 1 mL of 0.1 nM Au@SiO_2-CdTe@dBSA-NR colloidal solution was added to each solution, respectively. All of the mixed solutions were shaken for 2 min for the measurement. The size distribution of all the mixed solutions was also measured.

The response of 62.8 nm Au NSs, Au-62.8@SiO_2, Au-62.8@SiO_2-CdTe NPs with nitrite ions was performed, respectively. Briefly, 1 mL of 5 mM NO_2^- aqueous solutions and 1 mL of water (as control group) were prepared, respectively. Then 1 mL of 0.1 nM 62.8 nm Au NSs, Au-62.8@SiO_2 and Au-62.8@SiO_2-CdTe colloidal solution was added to each solution, respectively. All of the mixed solutions were shaken for 2 min before the measurement.

2.8 NO_2^- detection in real samples and cells supernatants

Real samples including local lake water, tap water and bacon lixivium by triturating bacon in aqueous solution were prepared, respectively. The samples were filtrated through a 0.45 μm membrane filter to remove the turbidity of particles. 1 mL of 0.1 nM Au@SiO_2-CdTe@dBSA-NR colloidal solution was then added to 1 mL of lake water, tap water and bacon lixivium, respectively. Each mixed solution was shaken 2 minutes for the measurement.

The RAW 264.7 cell lines were chosen for the NO_2^- detection in cells supernatants. Briefly, the RAW 264.7 cells were plated in 6-well plates at 1×10^6/well 24 h before the detection. 2 mL of serum-containing media were added to the cells and cultivated for 12 h. The cells were subsequently washed three times with phosphate buffer solution (PBS). Then 2 mL of serum-free media and 200 μL of 1 μg/mL LPS (NO inducing factor) or 200 μL of PBS buffer (as control group) were added to the cells and cultivated for another 12 h. The cells supernatant were collected after centrifugation and diluted 10-fold with PBS buffer. The NO_2^- detection in cells supernatants was performed using the procedure as follows.

The NO_2^- detection with Griess reaction: Briefly, 50 μL of Griess Reagent I and 50 μL of Griess Reagent II were added to 1 mL of the original supernatant solution and 10-fold diluted supernatant solution of both groups, respectively. All of the solutions were diluted to 2 mL for the measurement.

The NO_2^- detection with Au@SiO_2-CdTe@dBSA-NR fluorescent nanoprobe: Briefly, 1 mL of 0.1 nM Au@SiO_2-CdTe@dBSA-NR colloidal solution was added to 1 mL of the original supernatant solution and 10-fold diluted supernatant solution of both groups, respectively.

2.9 Characterization

The size and morphology were characterized by a Transmission Electron Microscope (TEM) (JEM-2100, JEOL, Tokyo, Japan) operated at an accelerating voltage of 200 kV. Absorption spectra were acquired with a DU 800 UV-Vis spectrophotometer (Beckman Coulter, Fullerton, CA). Fluorescence emission spectra were obtained by FluoroMax-4 spectrofluorometer (HORIBA Jobin Yvon, Palaiseau, France). The particles size distribution and Zeta potentials were measured with Nano-ZS ZEN3600 (Malvern, England).

3. Results and discussion

3.1 Characterization of Au NSs with different size and Au@SiO_2-CdTe NPs

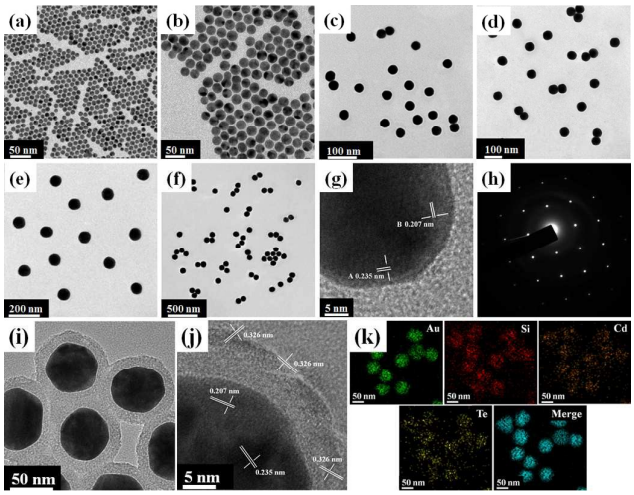

Fig. 1 TEM images of Au NSs with different size: (a) seeds with 10.9 nm in diameter, (b)-(f) 22.2, 40.5, 62.8, 81.8 and 103.8 nm in diameter, respectively, (g) HRTEM image and (h) selected area electron diffraction pattern of 22.2 nm Au NSs, (i) TEM image, (j) HRTEM image and (k) EDS element mappings of typical Au@SiO_2-CdTe NPs with 62.8 nm Au NSs.

TEM images of Au NSs with different size (Fig. 1a-f) illustrated that the obtained Au NSs were typically spherical, monodisperse and homogeneous with different average size nearly at 10.9, 22.2, 40.5, 62.8, 81.8 and 103.8 nm, respectively. As shown in Fig. S1, the mean hydrodynamic size of Au NSs in aqueous solution were 13.2±2.5, 25.3±2.8, 45.7±3.3, 65.5±3.7, 85.4±4.1 and 107.6±5.3 nm, respectively, matching well with the TEM images in Fig. 1. High resolution transmission electron microscope (HRTEM) image (Fig. 1g) and the selected area electron diffraction (SAED) pattern (Fig. 1h) of 22.2 nm Au NSs revealed that Au NSs were single crystalline. TEM image of TGA-capped CdTe QDs in aqueous solution (Fig. S2a) showed the synthesized CdTe QDs were monodisperse with a mean diameter of 2.45 nm. The SPR and emission peak wavelength of CdTe QDs (Fig. S2b) were 506 nm and 543 nm, respectively. Thus, the following fluorescence spectra were excited at 440 nm and collected from 450 nm to 800 nm.

The TEM image and HRTEM image of typical Au@SiO_2-CdTe NPs with 62.8 nm Au NSs (Au-62.8@SiO_2-CdTe NPs) were shown in Fig. 1i and Fig. 1j, respectively. The lattice spacing of the nanoparticles on the silica shell (Fig. 1j) was 0.326 nm, corresponding to the lattice of CdTe QDs (inset of Fig. S2a). Energy dispersive spectrometer (EDS) element mappings of Au, Si, Cd and Te were further performed to investigate the distribution of various

components (Fig. 1k). The results showed that CdTe QDs was successfully bound to Au-62.8@SiO_2 NPs. As a control, the physical mixture of CdTe QDs and Au-62.8@SiO_2 NPs was also characterized. The HRTEM image showed that CdTe QDs distributed around the Au-62.8@SiO_2 NPs randomly (Fig. S3a). Moreover, the fluorescence spectra of CdTe QDs, Au-62.8@SiO_2-CdTe NPs and CdTe QDs physically mixed with Au-62.8@SiO_2 NPs (Fig. S3b) illustrated that a 1.6-fold enhancement of fluorescence was obtained in the physical mixture of CdTe QDs and Au-62.8@SiO_2 NPs. This may be because MEF was working when partial CdTe QDs were nearly at the surface of Au-62.8@SiO_2 NPs.

The Au seed colloidal solution showed a surface plasmon resonance (SPR) peak at 520 nm (Fig. S4a). With the size of Au NSs increasing from 22.2 to 103.8 nm, the SPR peak of Au NSs with different size was noticeably red-shifted from 525 to 580 nm because the scattering effects of Au NSs became more relevant with the increasing of the size of Au NSs.[31] Digital photograph (Fig. S4b) showed the color of Au NSs colloidal solution with different size changed from red to wine red with the red-shifted of the SPR peak.

3.2 The size effect of Au NSs on MEF

Both the size of Au NSs and distance between QDs and Au NSs are considered as key factors affecting MEF.[32] Herein, we investigated the size effect of Au NSs on MEF. As shown in Fig. 2a-d, different Au NSs (size: 22.2, 40.5, 62.8 and 81.8 nm) were respectively coated with identical thickness (nearly 12 nm) of silica shell (labelled as Au-22.2@SiO_2, Au-40.5@SiO_2, Au-62.8@SiO_2 and Au-81.8@SiO_2, respectively). Fluorescence spectra of Au@SiO_2-CdTe with different size of Au NSs were shown in Fig. 2e. Obviously, fluorescence quenching was observed in Au-22.2@SiO_2-CdTe NPs, while fluorescence enhancement was observed in Au-40.5@SiO_2-CdTe, Au-62.8@SiO_2-CdTe and Au-81.8@SiO_2-CdTe NPs according to the enhancement factor (EF) calculation formula (1):

$$EF = \frac{I_i - I_{background}}{I_0 - I_{background}} \quad (1)$$

Where I_i is the fluorescence intensity of Au@SiO_2-CdTe colloidal solution with different size of Au NSs, $I_{background}$ is the fluorescence intensity of the blank solution and I_0 is the fluorescence intensity of CdTe QDs aqueous solution. As a result, the EF of Au-40.5@SiO_2, Au-62.8@SiO_2 and Au-81.8@SiO_2 to CdTe QDs was 1.2, 15.5 and 4.3, respectively. Thus Au-62.8@SiO_2-CdTe NPs was used throughout the following experiments.

According to Mie theory,[33] the size of Au NSs affects the absorption and scattering cross section of Au NSs in Au@SiO_2-CdTe NPs. Small colloidal Au NSs less than 40 nm in diameter, the absorption of which is dominant, are expected to quench the fluorescence of CdTe QDs. However, large colloidal Au NSs above 40 nm, the scattering of which becomes dominant, are expected to enhance the fluorescence of CdTe QDs. The scattering intensity increased gradually with the size increase of Au NSs, but the Mie extinction coefficient of Au NSs above 80 nm started to decrease. Thus, it is suggested that Au NSs with diameters between 40 nm and 80 nm were more efficient to enhance fluorescence. The amount of fluorescence enhancement was also depended on the spectral overlap between the LSPR of nanoparticle and the absorption and emission spectra of the dye.[34] Among the Au@SiO_2 NPs with different size of Au NSs in this paper, there was an optimal spectral overlap between the absorption spectrum of Au-62.8@SiO_2 NPs (535 nm) and the emission spectrum of CdTe QDs (543 nm). Therefore, the maximum fluorescence enhancement was achieved when the size of Au NSs was 62.8 nm and then started to decrease.

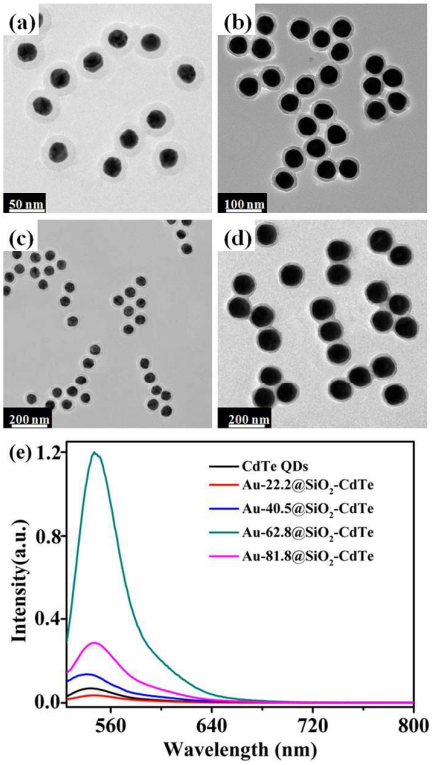

Fig. 2 TEM images of Au@SiO_2 with same thickness of silica shell (nearly 12 nm) and different size of Au NSs, (a)-(d): 22.2, 40.5, 62.8 and 81.8 nm, respectively, (e) Fluorescence spectra of Au@SiO_2-CdTe with different size of Au NSs excited at 440 nm.

3.3 The effect of the distance between Au NSs and CdTe QDs on MEF

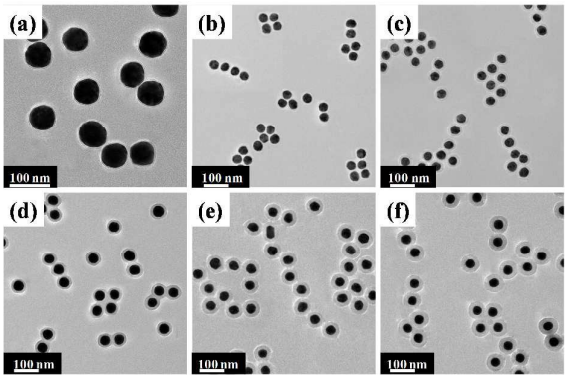

Fig. 3 TEM images of Au-62.8@SiO_2 NPs with different thickness of silica shell, (a)-(f): 2.1, 6.7, 12.5, 17.3, 21.5 and 26.7 nm, respectively.

The effect of the distance between Au NSs and CdTe QDs on MEF was also explored. The distance between Au NSs and CdTe QDs could be tuned by varying the thickness of silica shell, which was a facile approach to optimize the fluorescence enhancement. TEM images (Fig.3 a-f) showed Au-62.8@SiO_2 NPs with different thickness of silica shell from 2.1 to 26.7 nm (labelled as Au-62.8@SiO_2-2.1, Au-62.8@SiO_2-6.7, Au-62.8@SiO_2-12.5, Au-62.8@SiO_2-17.3, Au-62.8@SiO_2-21.5 and Au-62.8@SiO_2-26.7, respectively) by carefully changing the dose of silica precursor.

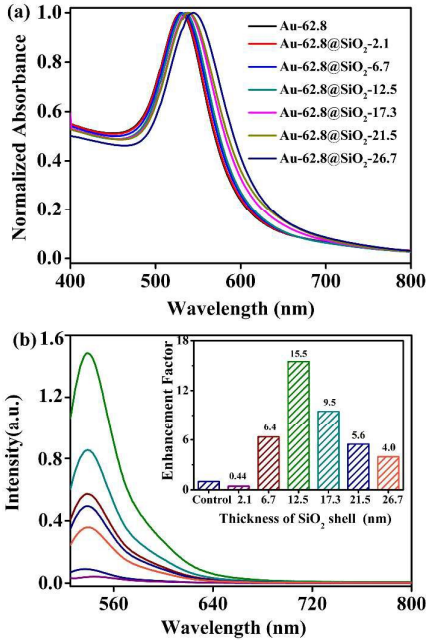

Fig. 4 (a) Normalized absorption spectra and (b) Fluorescence spectra of Au-62.8@SiO_2-CdTe NPs with different thickness of silica shell excited at 440 nm. Inset: fluorescence enhancement factors.

Normalized absorption spectra of Au-62.8@SiO_2 NPs with different thickness of silica shell (Fig. 4a) showed the SPR peak of Au-62.8 NSs was 530 nm. With the thickness of silica shell increasing from 2.1 to 26.7 nm, the SPR peak of Au-62.8@SiO_2 NPs was gradually red-shift from 530 to 545 nm. This phenomenon can be explained that the refractive index of silica shell is higher than that of water, and the increasing thickness of silica shell onto Au NSs led to the increasing of the local refractive index around Au NSs, resulting in red-shift of SPR peak.[35] Fluorescence spectra of Au-62.8@SiO_2-CdTe NPs with different thickness of silica shell (Fig. 4b) showed the EF for each kind of Au-62.8@SiO_2 to CdTe QDs was 0.4, 6.4, 15.5, 9.5, 5.6 and 4.0 according to the result of calculation (inset of Fig. 4b), respectively. Quenching effects are dominant when the thickness of silica shell is less than 5 nm, but MEF mechanisms, including resonance energy transfer (RET) and nearly field enhancement (NFE), are dominant when the thickness of silica shell is larger than 5 nm, resulting in the fluorescence enhancement of CdTe QDs. However, the MEF effect will reach the maximum when the thickness of silica shell is about 12 nm and then start to decrease.[36] Therefore, the fluorescence enhancement reached the maximum in Au-62.8@SiO_2-12.5-CdTe NPs.

3.4 Characterization of Au@SiO_2-CdTe@dBSA NPs

Table 1 Particle size distribution and zeta potentials of various NPs.

Sample	Hydrodynamic size(nm)	Zeta potential(mV)
CdTe QDs	4.5±0.9	-42.4±1.5
Au-62.8@SiO_2	87.5±2.7	-16.8±3.1
Au-62.8@SiO_2-NH_2	88.7±2.1	27.2±3.6
Au@SiO_2-CdTe	94.1±1.7	14.8±2.5
Au@SiO_2-CdTe@dBSA	98.7±2.4	-17.5±2.9

The particle size distribution and zeta potentials of CdTe QDs, Au-62.8@SiO_2, Au-62.8@SiO_2-NH_2, Au@SiO_2-CdTe and Au@SiO_2-CdTe@dBSA NPs in aqueous solution were shown in Table 1. The change of the size and Zeta potential from Au-62.8@SiO_2 to Au-62.8@SiO_2-NH_2 NPs indicated the APTMS was successfully modified on the surface of Au-62.8@SiO_2 NPs. The change of the size and Zeta potential from Au-62.8@SiO_2 to Au@SiO_2-CdTe NPs indicated the successful binding of CdTe QDs to Au-62.8@SiO_2 NPs. Similarly, the change of the size and zeta potential from Au@SiO_2-CdTe to Au@SiO_2-CdTe@dBSA NPs in aqueous solution proved the coating of dBSA.

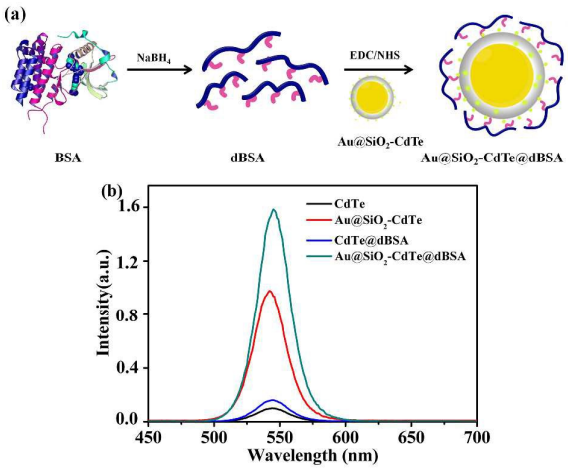

Fig. 5 (a) Schematic diagram for the formation process of Au@SiO_2-CdTe@dBSA NPs, (b) Fluorescence spectra of CdTe QDs, CdTe@dBSA, Au@SiO_2-CdTe and Au@SiO_2-CdTe@dBSA NPs excited at 440 nm.

dBSA was prepared by reducing BSA with $NaBH_4$ (Fig. 5a). Fluorescence spectra of CdTe QDs, CdTe@dBSA, Au@SiO_2-CdTe and Au@SiO_2-CdTe@dBSA NPs were shown in Fig. 5b, an obviously 1.6-fold fluorescence enhancement of Au@SiO_2-CdTe NPs was achieved by coating with dBSA, which can be explained that dBSA wraps on the surface of SiO_2 and CdTe QDs to form of a shell-like structure due to its multiple binding sites. Such a shell structure results in not only the removal of dangling bonds of Te atoms from the surface of CdTe QDs but also the formation of a thermodynamically stable core-shell-like structure, leading to a better confinement of photo-generated charge carriers.[30, 37] Thus, CdTe@dBSA and Au@SiO_2-CdTe@dBSA NPs exhibited higher stability and fluorescence quantum yield than CdTe QDs.

3.5 NO_2^- detection in aqueous solution

NR has been developed as a probe for NO_2^- detection.[25] NO_2^- selectively reacted with the primary aromatic amine group of NR to form a diazonium group in acidic media (Fig. 6a). The diazonium group would be unstable in weak acidic media and rapidly transformed to another product (named de-(NH_2) NR) by releasing nitrogen (N_2) at room temperature. NR molecules were positively charged thus they could be absorbed to Au@SiO_2-CdTe@dBSA NPs through charge interaction. Moreover, the absorption spectrum of NR had well overlap with the fluorescence spectrum of CdTe QDs (Fig. 6b), which ensured resonant interaction between NR and CdTe QDs.

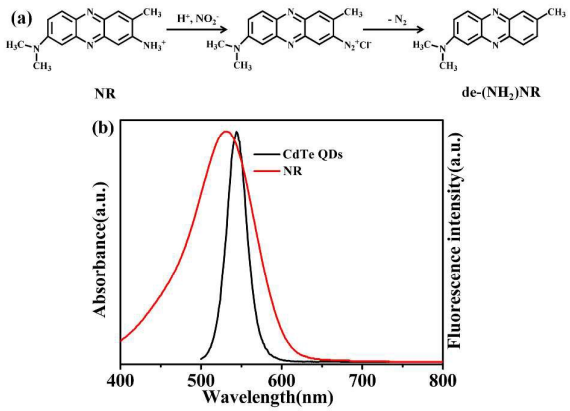

Fig. 6 (a) The reaction between NR and NO_2^-, (b) Absorption spectrum of NR (red line) and fluorescence spectrum of CdTe QDs excited at 440 nm (black line).

The reaction between Au@SiO_2-CdTe@dBSA-NR fluorescent nanoprobe and NO_2^- could be clearly monitored by fluorescence spectra. With an increasing concentration of NO_2^- ranging from 0 to 25 μM, the green emission at 543 nm of CdTe QDs was continuously recovered and the red emission at 621 nm of NR was gradually quenched (Fig. 7a). The fluorescence intensity ratio (I_{543}/I_{621}) showed a good linear correlation with the concentration of NO_2^- (Fig. 7b), which could be chosen as a detection signal. The linear regression could be described by the following equation (2):

$$I_{543} / I_{621} = 0.153C + 0.573 \quad (2)$$

Where C was the concentration of NO_2^- in $\times 10^{-6}$ M, and the correlation coefficient was 0.994. The detection limit (3σ) of NO_2^- with Au@SiO_2-CdTe@dBSA-NR fluorescent nanoprobe was found to be as low as 60 nM, much lower than the detection limit of NO_2^- with NR (15μM) in previous work.[25]

The detection mechanism of NO_2^- with Au@SiO_2-CdTe@dBSA-NR fluorescent nanoprobe was shown in Fig. 7c. For the FRET pairs in Au@SiO_2-CdTe@dBSA-NR fluorescent nanoprobe, CdTe QDs were the donor and NR was the acceptor, respectively. Firstly, NR was adsorbed onto the surface of Au@SiO_2-CdTe@dBSA, resulting in the red emission of NR at 621 nm and the quenching of the green emission of CdTe QDs at 543 nm due to the FRET from CdTe QDs to NR. In the presence of NO_2^-, NR transformed to de-(NH_2) NR, leading to the great decrease of spectral absorption of NR at 531 nm and detaching from Au@SiO_2-CdTe@dBSA NPs. Thus the path way of energy transfer between NR and CdTe QDs was shut off and then the green emission of CdTe QDs gradually recovered. It could be inferred that the recovery of the green emission of CdTe QDs was depended on the ratio of residual NR to de-(NH_2) NR in the detection solution. Therefore, the fluorescence spectral change responded to the amount of de-(NH_2) NR, which provided a spectral detection of NO_2^-.

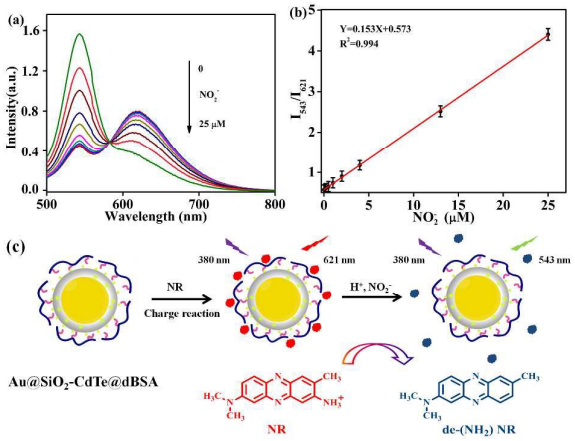

Fig.7 (a) Fluorescence spectra of Au@SiO_2-CdTe@dBSA-NR fluorescent nanoprobe excited at 440 nm and (b) The linear regression curve of I_{543}/I_{621} towards the concentration of NO_2^-, (c) The detection mechanism of NO_2^- with Au@SiO_2-CdTe@dBSA-NR fluorescent nanoprobe.

3.6 Selectivity assay towards NO_2^-

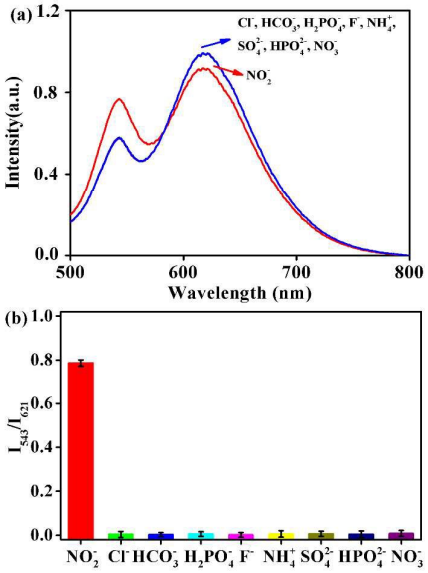

Fig. 8 (a) Fluorescence spectra of Au@SiO_2-CdTe@dBSA-NR fluorescent nanoprobe excited at 440 nm towards NO_2^- and other representative ions, (b) The fluorescence intensity ratio (I_{543}/I_{621}) of Au@SiO_2-CdTe@dBSA-NR fluorescent nanoprobe in response to NO_2^- and other representative ions.

To study the selectivity of Au@SiO_2-CdTe@dBSA-NR fluorescent nanoprobe towards the detection of NO_2^- over other

representative ions, 100-fold concentration of other ions including Cl^-, HCO_3^-, $H_2PO_4^-$, F^-, NH_4^+, SO_4^{2-}, HPO_4^{2-} and NO_3^- were incubated with Au@SiO_2-CdTe@dBSA-NR fluorescent nanoprobe. As shown in Fig. 8a, negligible fluorescence spectral change was observed towards even 100-fold concentration of other ions. However, only NO_2^- led to the quenching of the red emission of NR at 621 nm and the recovery of the green emission of CdTe QDs at 543 nm due to the specific reaction between NO_2^- and NR, corresponding to the detection of NO_2^- in aqueous solution. In addition, the value of I_{543}/I_{621} could also confirm the selectivity of detection that the I_{543}/I_{621} towards NO_2^- was much higher than that for other ions (Fig. 8b). Thus, the as-prepared fluorescent nanoprobe exhibited an excellent selectivity for the detection of NO_2^-.

To study the stability of fluorescent nanoprobe in the ionic solution, the particle size distribution of the ionic solutions added with fluorescent nanoprobe were measured. Obviously, negligible aggregation was observed according to the DLS data (Fig. S5), because of the numerous negative charge of dBSA coated onto the fluorescent nanoprobe. Therefore, the fluorescent nanoprobe was stable in the ionic solution.

The response of 62.8 nm Au NSs, Au-62.8@SiO_2, Au-62.8@SiO_2-CdTe NPs with nitrite ions independently were also performed to explore the selectivity of the fluorescent nanoprobe . As shown in Fig. S6, there was no obvious difference in the absorption spectra of Au and Au-62.8@SiO_2 NPs and the fluorescence spectra of Au-62.8@SiO_2-CdTe NPs when detected NO_2^- or water, respectively, indicating that these nanoparticles didn't exhibit a selectivity towards NO_2^-. It was further confirmed that the excellent selectivity of Au@SiO_2-CdTe@dBSA-NR fluorescent nanoprobe for the detection of NO_2^- was owing to neutral red (NR).

3.7 NO_2^- detection in real samples and cells supernatants

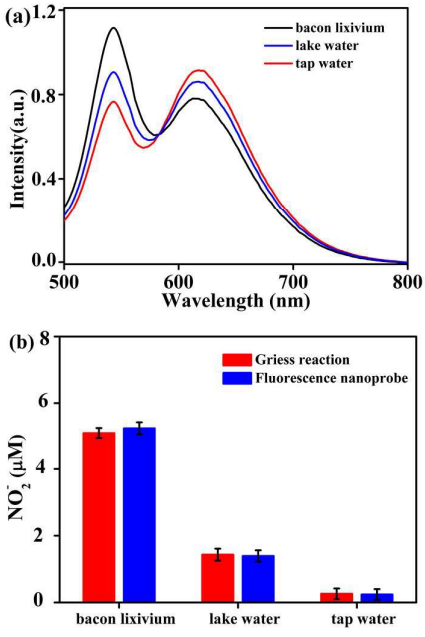

Fig. 9 (a) Fluorescence spectra for the detection of NO_2^- in real samples with Au@SiO_2-CdTe@dBSA-NR fluorescent nanoprobe excited at 440 nm, (b) NO_2^- detection in real samples with Griess reaction and Au@SiO_2-CdTe@dBSA-NR fluorescent nanoprobe.

The potential application of NO_2^- detection with Au@SiO_2-CdTe@dBSA-NR fluorescent nanoprobe was explored in real samples including tap water, bacon lixivium and lake water. Griess reaction, as a conventional method for the detection of NO_2^-,[4, 38] was set as control group. As shown in Fig. 9, the concentration of NO_2^- in lake water, bacon lixivium and tap water were measured at 1.5 μM, 5.1 μM and 0.2 μM, respectively (Fig. 9b) with Au@SiO_2-CdTe@dBSA-NR fluorescent nanoprobe. The result was in good agreements when detecting bacon lixivium, lake water and tap water with Griess reaction or Au@SiO_2-CdTe@dBSA-NR fluorescent nanoprobe. The satisfactory results demonstrated that Au@SiO_2-CdTe@dBSA-NR fluorescent nanoprobe was suitable for its application in real samples with high sensitivity.

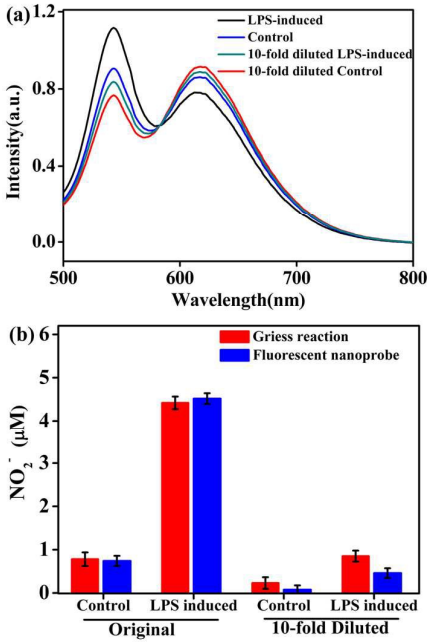

Fig. 10 (a) Fluorescence spectra of the detection of NO_2^- in cells supernatants with Au@SiO_2-CdTe@dBSA-NR fluorescent nanoprobe excited at 440 nm, (b) NO_2^- detection in cells supernatants with Au@SiO_2-CdTe@dBSA-NR fluorescent nanoprobe and Griess reaction.

NO, easily oxidized to NO_2^- in aqueous solution,[4] plays an important role in a number of signaling pathways and immune responses. The potential application of NO_2^- detection with Au@SiO_2-CdTe@dBSA-NR fluorescent nanoprobe was also explored in cells supernatants. LPS, as a stimulator for immune response, is used to induce the NO generation of the RAW 264.7 cells.[39, 40] Fluorescence spectra of the detection of NO_2^- in cells supernatants with Au@SiO_2-CdTe@dBSA-NR fluorescent nanoprobe showed that the concentration of NO_2^- in LPS-induced cells supernatant was 5.6-fold than that of the control group, which was in good agreement with Griess reaction (Fig. 10a, b). However, NO_2^- could also be detected with Au@SiO_2-CdTe@dBSA-NR fluorescent nanoprobe even in 10-fold diluted cells supernatants, which could not be accurately quantified by Griess method. The

results above demonstrated that Au@SiO_2-CdTe@dBSA-NR fluorescent nanoprobe owned the ability of trace detection of NO_2^- when compared with conventional Griess reaction.

4. Conclusions

In summary, a novel Au@SiO_2-CdTe@dBSA-NR fluorescent nanoprobe based on MEF combined with FRET has been developed and demonstrated for the trace detection of NO_2^-. The as-prepared Au@SiO_2-CdTe@dBSA-NR fluorescent nanoprobe exhibited high selectivity, sensitivity and low detection limit of NO_2^- (60 nM) in the detection of NO_2^- concentration in real samples including tap water, bacon lixivium and lake water and in LPS-induced RAW 264.7 cells supernatant. The present fluorescent nanoprobe provides a new strategy to detect NO_2^- with high selectivity and low detection limit and therefore is expected to use for the analysis of NO_2^- in various applications.

Acknowledgements

This work was financially supported by the National Basic Research Program of China (973 Program) (2013CB933703), the National Natural Science Foundation of China (Nos. 31371012, 31428007, U1505228).

References

1. N. Dai and W. A. Mitch, *Environmental science & technology*, 2013, **47**, 3648-3656.
2. D. Bellin, S. Asai, M. Delledonne and H. Yoshioka, *Molecular plant-microbe interactions*, 2013, **26**, 271-277.
3. B. B. Mishra, V. A. Rathinam, G. W. Martens, A. J. Martinot, H. Kornfeld, K. A. Fitzgerald and C. M. Sassetti, *Nature immunology*, 2013, **14**, 52-60.
4. P. N. Coneski and M. H. Schoenfisch, *Chemical Society Reviews*, 2012, **41**, 3753-3758.
5. Z. Lin, W. Xue, H. Chen and J.-M. Lin, *Analytical chemistry*, 2011, **83**, 8245-8251.
6. H. Liu, G. Yang, E. Abdel-Halim and J.-J. Zhu, *Talanta*, 2013, **104**, 135-139.
7. D. Tsikas, A. Schwarz and D. O. Stichtenoth, *Analytical chemistry*, 2010, **82**, 2585-2587.
8. L. He, K. Zhang, C. Wang, X. Luo and S. Zhang, *Journal of Chromatography A*, 2011, **1218**, 3595-3600.
9. X. Wang, E. Adams and A. Van Schepdael, *Talanta*, 2012, **97**, 142-144.
10. S. Radhakrishnan, K. Krishnamoorthy, C. Sekar, J. Wilson and S. J. Kim, *Applied Catalysis B: Environmental*, 2014, **148**, 22-28.
11. J. Li, Q. Li, C. Lu and L. Zhao, *Analyst*, 2011, **136**, 2379-2384.
12. J. Han, C. Zhang, F. Liu, B. Liu, M. Han, W. Zou, L. Yang and Z. Zhang, *Analyst*, 2014, **139**, 3032-3038.
13. M. Saboktakin, X. Ye, S. J. Oh, S.-H. Hong, A. T. Fafarman, U. K. Chettiar, N. Engheta, C. B. Murray and C. R. Kagan, *ACS nano*, 2012, **6**, 8758-8766.
14. J. Yang, F. Zhang, Y. Chen, S. Qian, P. Hu, W. Li, Y. Deng, Y. Fang, L. Han and M. Luqman, *Chemical Communications*, 2011, **47**, 11618-11620.
15. Y. Tang, Q. Yang, T. Wu, L. Liu, Y. Ding and B. Yu, *Langmuir*, 2014, **30**, 6324-6330.
16. Y.-Q. Li, L.-Y. Guan, H.-L. Zhang, J. Chen, S. Lin, Z.-Y. Ma and Y.-D. Zhao, *Analytical chemistry*, 2011, **83**, 4103-4109.
17. W. Ge, X. Zhang, M. Liu, Z. Lei, R. Knize and Y. Lu, *Theranostics*, 2013, **3**, 282.
18. M. Xue, X. Wang, L. Duan, W. Gao, L. Ji and B. Tang, *Biosensors and Bioelectronics*, 2012, **36**, 168-173.
19. M. Xue, X. Wang, H. Wang, D. Chen and B. Tang, *Chemical Communications*, 2011, **47**, 4986-4988.
20. J. Asselin, M. L. Viger and D. Boudreau, *Advances in Chemistry*, 2014, **2014**.
21. S. T. Kochuveedu, T. Son, Y. Lee, M. Lee, D. Kim and D. H. Kim, *Scientific reports*, 2014, **4**.
22. W. Zhang, X.-W. He, Y. Chen, W.-Y. Li and Y.-K. Zhang, *Biosensors and Bioelectronics*, 2012, **31**, 84-89.
23. J. Sun, L. Guo, H. Xu, J. Tang and J. Xie, *Biosensors and Bioelectronics*, 2013, **43**, 446-452.
24. B. Narayana and K. Sunil, *Eurasian Journal of Analytical Chemistry*, 2009, **4**, 204-214.
25. N. Gayathri and N. Balasubramanian, *Analusis*, 1999, **27**, 174-180.
26. G. Frens, *Nature*, 1973, **241**, 20-22.
27. J. Niu, T. Zhu and Z. Liu, *Nanotechnology*, 2007, **18**, 325607.
28. Y. Lu, Y. Yin, Z.-Y. Li and Y. Xia, *Nano Letters*, 2002, **2**, 785-788.
29. N. Gaponik, D. V. Talapin, A. L. Rogach, K. Hoppe, E. V. Shevchenko, A. Kornowski, A. Eychmüller and H. Weller, *The Journal of Physical Chemistry B*, 2002, **106**, 7177-7185.
30. Q. Wang, Y. Kuo, Y. Wang, G. Shin, C. Ruengruglikit and Q. Huang, *The Journal of Physical Chemistry B*, 2006, **110**, 16860-16866.
31. J. Rodríguez-Fernández, J. Pérez-Juste, F. J. García de Abajo and L. M. Liz-Marzán, *Langmuir*, 2006, **22**, 7007-7010.
32. N. Liu, B. S. Prall and V. I. Klimov, *Journal of the American Chemical Society*, 2006, **128**, 15362-15363.
33. P. K. Jain, K. S. Lee, I. H. El-Sayed and M. A. El-Sayed, *The Journal of Physical Chemistry B*, 2006, **110**, 7238-7248.
34. Y. Chen, K. Munechika and D. S. Ginger, *Nano letters*, 2007, **7**, 690-696.
35. T. Ung, L. M. Liz-Marzan and P. Mulvaney, *The Journal of Physical Chemistry B*, 2001, **105**, 3441-3452.
36. Y. Fu, J. Zhang and J. R. Lakowicz, *Journal of the American Chemical Society*, 2010, **132**, 5540-5541.
37. Y.-C. Kuo, Q. Wang, C. Ruengruglikit, H. Yu and Q. Huang, *The Journal of Physical Chemistry C*, 2008, **112**, 4818-4824.
38. K. M. Miranda, M. G. Espey and D. A. Wink, *Nitric oxide*, 2001, **5**, 62-71.
39. H.-Y. Lin, S.-H. Juan, S.-C. Shen, F.-L. Hsu and Y.-C. Chen, *Biochemical pharmacology*, 2003, **66**, 1821-1832.
40. C. Moro, I. Palacios, M. Lozano, M. D'Arrigo, E. Guillamón, A. Villares, J. A. Martínez and A. García-Lafuente, *Food Chemistry*, 2012, **130**, 350-355.

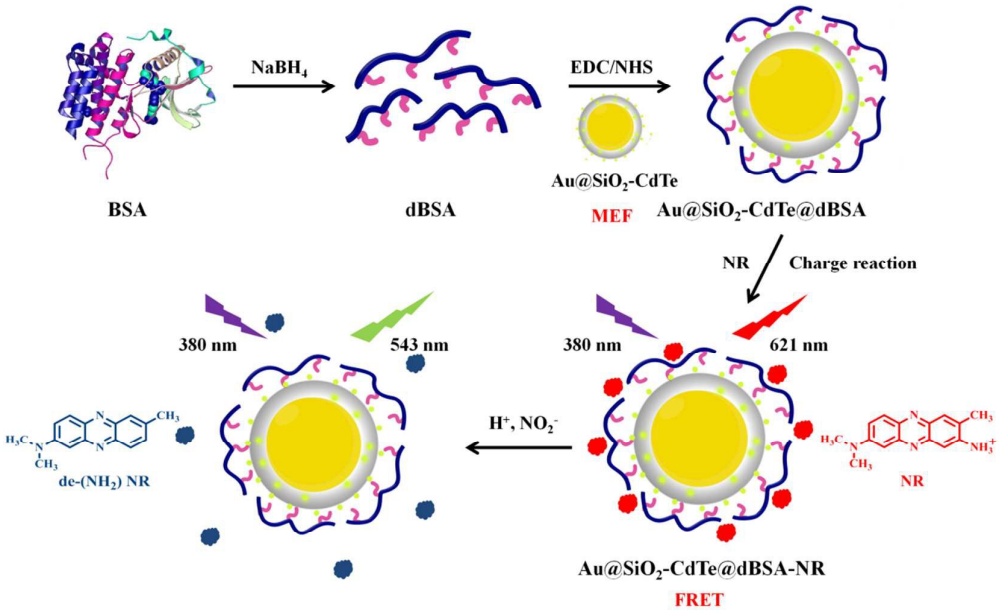

Graphic abstract: The schematic diagram of the synthesis of $Au@SiO_2$-CdTe@dBSA-NR fluorescent nanoprobe and the detection mechanism for NO_2^-

Highlight: Fluorescent nanoprobe utilizing metal enhanced fluorescence (MEF), Förster resonance energy transfer (FRET) and coating with denatured bovine serum albumin (dBSA)